Liver Tumour Classification based on DCE-MRI Images

Nuno Barros*and João Sanches

Institute for Systems and Robotics / Instituto Superior Técnico
Lisboa, Portugal

Abstract

This paper presents a description of a method for modeling liver pharmokinetics and retrieving tumor perfusion data using DCE-MRI images. This tumor perfusion information is assessed with the purpose of classifying liver tumors in terms of its malignancy.

Six multiphasic DCE-MRI abdominal studies, with confirmed diagnosis (5 malignant out of 9 tumors), were analyzed using the method described. These imaging studies contained a total of 9 tumors, including 4 benign tumors and 5 carcinomas. Considering the results obtained, the arterial ratio was the parameter that allowed a better distinction between benign and malign lesions.

Besides using low temporal images, the results confirmed the fact of liver carcinomas being mostly supplied by the hepatic artery. Benign tumors registered mean arterial ratios between 16.6% and 37.5%. On the other hand, malignant tumors revealed an arterial component in a range between 51.4% and 75.5%.

1 Introduction

According to the IARC(International Agency for Research on Cancer) Globocan 2008 project, liver cancer killed 478,275 persons worldwide and 522,355 new cases were registered in 2008. This proximity between incidence and mortality values reveals how deadly liver cancer is. In order to improve the survival of this disease, liver cancer has to be detected in an early stage, when due to its smaller dimensions and less marked features its identification is more difficult.

Dynamic Contrast Enhanced Magnetic Resonance Imaging (DCE-MRI) has proven to be the most efficient diagnose method for liver tumor identification([3],[10],[12]). Moreover, its capabilities can be considerably improved by modeling the imaging data with pharmokinetic models that describe the contrast diffusion process. The application of such models allows retrieving diverse perfusion information.

Presently, many sorts of contrast agents are available for DCE-MRI. Normally, low molecular weight Gadolinium chelates are used. After the injection of this type of contrast agents, their molecules are found diffused in the blood plasma. When the blood reaches the capillaries, the thin revestment layer allows the passage of these molecules into the Extravascular Extracellular Space (EES). The process of contrast diffusion, between the blood plasma and the EES, depends on the corresponding concentration difference, blood flow and permeability characteristics.

The liver is characterized by a dual-blood supply, where about 75% of the blood has its origin in the hepatic portal vein and the rest 25% in the hepatic artery. However, tissue arterial ratio, as other perfusion characteristics, is altered in several pathological conditions, such as liver cancer.

2 Imaging Data

The multiphasic DCE-MRI studies used included six images each. The first image corresponds to the non-contrast acquisition, the following three to the arterial phase acquired using the keyhole technique, the fifth one to the portal phase and the last one to the equilibrium phase.

All imaging studies were acquired with a 1.5 Tesla superconducting magnet (Philips Achieva; Hospital Erasme, Brussels) with the patients placed in the supine position. A T1-weighted Gradient Echo sequence was used with a flip angle of 10º, repetition time of 3.93 msec and echo time of 1.87 msec.

A low weight extracellular contrast - Gadovist 1.0M - was injected in a peripheral vein.

In terms of fat suppression, Spectral Adiabatic Inversion Recovery (SPAIR) was used.

Each image had the following matrix dimensions: 256x256x150; with a corresponding pixel spacing of 1.75 mm, a slice thickness of 3.6 mm and spacing between slices of 1.8 mm.

3 Method

In order to be able to proceed with a pharmacokinetic analysis, a relation between intensity and contrast concentration should be established. The best way to do this is by previous calibration, filling several tubes with different solutions of known contrast concentrations and imaging them [5]. Unfortunately, this information was not known. Even so, some studies point a linear relation between contrast concentration and relaxivity[9]. Considering this, contrast concentration can be approximated by the relative signal, or:

$$C(t, x, y, z) \approx \frac{I(t, x, y, z) - I(0, x, y, z)}{I(0, x, y, z)} \tag{1}$$

, where $C(t, x, y, z)$ is the contrast concentration at time t in the voxel with coordinates (x, y, z); and $I(t, x, y, z)$ is the intensity value of the same voxel at the same time.

The model to be used should consider the path of contrast substance since the bolus injection until it reaches the hepatocytes. Moreover, in order to be able to resolve arterial and portal components for each voxel, the hepatic dual-blood supply should be considered. The overall process of contrast diffusion can then be modeled as shown in figure 1.
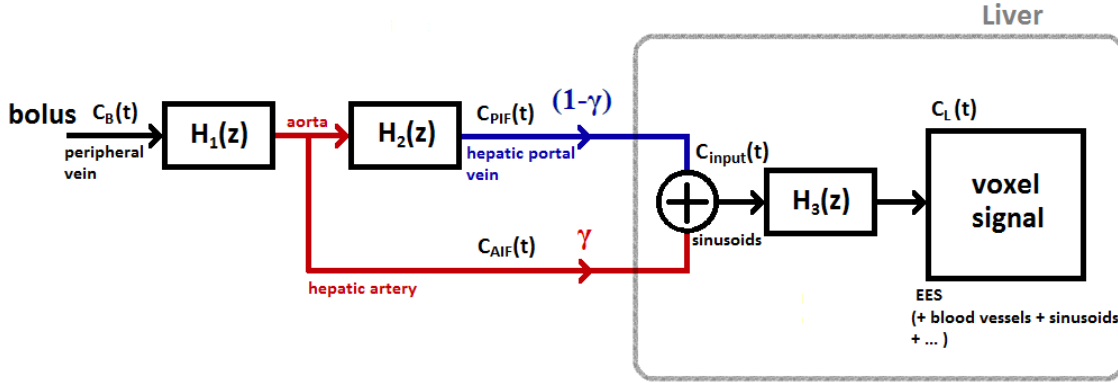

Figure 1. *Pharmacokinetic model used.*

The Arterial Input Function (AIF) may be defined considering that the concentration in blood plasma is the superposition of the bolus shape and its shape after modification by the body impulse response[6]:

$$C_{AIF}(t) = C_B(t) + C_B(t) \otimes G(t) \tag{2}$$

, being $C_B(t)$ the bolus function; $C_{AIF}(t)$ the AIF or mean contrast concentration in the aorta at time t; and $G(t)$ the body impulse response. Here $G(t)$ represents the transfer function corresponding to the diffusion processes that occur between the bolus injection in a peripheral vein and the aorta. The model assumes that the signal is the same in the aorta and hepatic artery.

If we now consider a bolus of the form:

$$C_B(t) = \begin{cases} 0 & \text{if t=0} \\ a_B t e^{-\mu_B t} & \text{if t>0} \end{cases} \tag{3}$$

, and a body impulse response $G(t) = a_G e^{-\mu_G t}$, we obtain the following AIF:

$$C_{AIF}(t) = A_B t e^{-\mu_B t} + A_G (e^{-\mu_G t} - e^{-\mu_B t}) \tag{4}$$

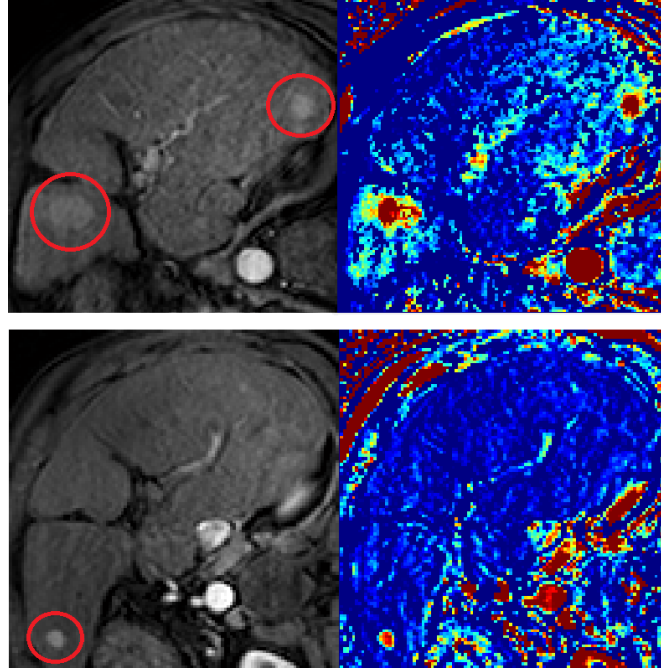, with $A_B = a_B - a_B a_G / (\mu_B - \mu_G)$ and $A_G = a_B a_G / (\mu_B - \mu_G)$.

Figure 2. *Whole liver arterial ratio analysis (right side). In the left side is presented the MR image slice where the tumor limits where more easily identified (arterial phase). The tumors (Hepatocellular Carcinoma) are signaled with a red circle.*

The contrast collected by the hepatic portal vein from the gastrointestinal tract is found previously in the aorta. As so, the Portal Input Function (PIF) may consider the AIF as input. The corresponding contrast transference may be modeled using the Tofts *et al.* generalized kinetic model[11], as an example of a flow limited situation:

$$C_{PIF}(t) = K_{AP}^{trans} C_{AIF}(t) \otimes e^{-k_P(t-\tau_1)} \tag{5}$$

, where C_{PIF} is the PIF or mean contrast concentration in the portal vein at time t, K_{AP}^{trans} is related to blood flow between the two regions; k_P characterizes the speed of the process; and τ_1 corresponds to the time taken by the contrast to travel from the aorta to the hepatic portal vein.

In the liver, the blood from the two distinct sources is mixed and passes through the sinusoids, where part of the contrast is retained in the space of Disse. After the sinusoids, the blood is collected by the hepatic vein. Considering this, the contrast concentration found in one liver voxel $C_L(t)$ may be given by:

$$C_L(t) = K_L^{trans} C_{input}(t) \otimes e^{-k_L(t-\tau_2)} \tag{6}$$

, where K_L^{trans} is related to liver blood flow and sinusoidal walls permeability, k_L is a parameter connected to the speed of contrast diffusion, τ_2 represents the delay gained between the regions where the input functions are measured and the observed voxel, and $C_{input}(t)$ is the input function, given by the weighted sum of the AIF and PIF:

$$C_{input}(t) = \gamma C_{AIF}(t) + (1 - \gamma) C_{PIF}(t) \tag{7}$$

, being γ the arterial ratio.

The application of the model starts with the definition of the input functions. This is done by fitting the expressions in equations (4) and (5) to the mean relative intensity of two pre-defined ROI in the aorta and hepatic portal vein. Then the algorithm starts calculating the perfusion curves voxel-by-voxel, fitting the equation (6) to the six relative intensity points of each voxel. The fitting processes are performed using a least-squares approach.

4   Results

The complete set of parameters obtained for each tumor is attached to this paper. As it can be seen, the arterial ratio revealed to be superior, in terms of malignancy detection, in comparison with other parameters. However this result should be explained by the use of low resolution studies; taking into account that the type of analysis made here is normally applied to images acquired continuously with higher temporal resolution. Nevertheless, perfusion anomalies were detected in all tumors and the results obtained for the arterial rate are in accordance with the typical characteristics of the development of liver carcinomas.

Figure 2 shows two arterial ratio maps of entire slices of the liver. The examples given include three tumors and demonstrate the usefulness of the arterial ratio in tumor detection. The parameter maps were compared with the DCE-MRI image where the tumors were more easily identified.

Patient	Tumor	Path.	Ben./ Malig.	Volume (cm^3)	Diam. (cm)	Arterial ratio	std	Tum. Mean Perf. Vol.	Liv. Mean Perf. Vol.	Perf. ratio (Tum./Liv.)
1		Met	M	35.12	4.06	0.608	0.471	7.03	15.55	0.45
2	1	NRH	B	326.33	8.54	0.202	0.206	116.10	26.16	4.44
2	2	NRH	B	3.07	1.80	0.168	0.166	117.76	26.16	4.50
3		FNH	B	6.26	2.29	0.375	0.245	152.88	88.69	1.72
4		Hem	B	17.49	3.22	0.166	0.208	263.23	85.62	3.07
5	1	HCC	M	73.28	5.19	0.660	0.422	21.68	86.04	0.25
5	2	HCC	M	0.93	1.21	0.736	0.175	147.35	86.05	1.71
5	3	HCC	M	2.40	1.66	0.755	0.211	146.29	86.05	1.70
6		HCC	M	25.11	3.63	0.514	0.362	86.18	36.32	2.37

Table 1. *Summary table of the most relevant parameters in a tumor classification perspective. The mean tumor arterial ratios are shown together with the corresponding standard deviation (std). The tumor mean diameter was calculated considering a perfect sphere. The calculation of the tumor dimensions considered the voxel dimensions and spacing between slices. Pathology abbreviations used: Met - Metastase; NRH - Nodular Regenerative Hyperplasia; FNH - Focal Nodular Hyperplasia; Hem - Hemangioma; HCC - Hepatocellular Carcinoma*.

In figure 3 is shown a comparison between an arterial ratio map of a benign tumor and a carcinoma. Here is visible the highest arterial component characteristic of malignant tissue. The most relevant results obtained for all tumors are resumed in table 1. As it can be observed, there were detected clear difference between benign and malignant tumors in terms of the arterial ratio.

In table 1, the perfusion volume values represent simply the integral of the perfusion curves. Consequently they depend on the time of acquisition, as well as on the time at which the contrast was injected, what jeopardizes a inter-tumoral comparison of these values. As a result, it was introduced the liver perfusion volume in order to allow the calculation of the corresponding tumor/liver ratio. A greater ratio value should mean that, in comparison with the liver, more contrast is detected in that tissue during the same time. This is related to the contrast uptake and residence time.

Overall, the referred ratio was smaller in the malignant tumors. This may express a higher wash-out rate in malignant tumors and a perfusion decrease especially in larger ones. More tests should be performed with the purpose of determining the ability of this ratio to help in tumor characterization. In terms of the big carcinomas found in patient 1 and 5, the small ratio values may reveal the presence of necrotic tissue.
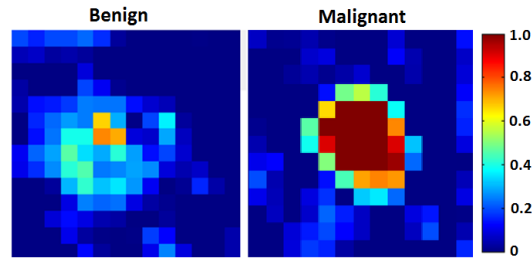
Figure 3. *Comparison example between two arterial ratio maps from one slice of one benign tumor(Focal Nodular Hyperplasia - Patient 3) and one malignant tumor(Hepatocellular Carcinoma - Patient 5, Tumor 3)*.

5 Conclusion

The model presented was able to detect clear differences, in terms of the arterial ratio, between benign and malignant liver tumors. Despite this ratio having been the most capable of malignancy detection, the use of higher temporal resolution cases may put into evidence other perfusion differences and provide more accurate arterial ratio results. This increased accuracy may allow noninvasive quantitative perfusion measurements. Moreover, in a near future this information may be shared by several hospitals and used towards automatic tumor classification.

In short, the results have highlighted the usefulness of pharmokinetic analysis in liver cancer diagnosis, namely by resolving arterial and hepatic portal venous components.

References

[1] S. Aime and P. Caravan. Biodistribution of gadolinium-based contrast agents, including gadolinium deposition. *Journal of Magnetic Resonance Imaging*, 30(6):1259–1267, 2009.

[2] L. Caldeira and J. Sanches. Pharmacokinetic Perfusion Curves Estimation for Liver Tumor Diagnosis from DCE-MRI. *Image Analysis and Recognition*, pages 789–797, 2008.

[3] S. Digumarthy, D. Sahani, and S. Saini. MRI in detection of hepatocellular carcinoma (HCC). *Cancer Imaging*, 5(1):20, 2005.

[4] A. Jackson, D. Buckley, and G. Parker. *Dynamic contrast-enhanced magnetic resonance imaging in oncology*. Springer-Verlag Berlin Heidelberg, 2005.

[5] R. Materne, A. Smith, F. Peeters, J. Dehoux, A. Keyeux, Y. Horsmans, and B. Van Beers. Assessment of hepatic perfusion parameters with dynamic MRI. *Magnetic Resonance in Medicine*, 47(1):135–142, 2002.

[6] M. Orton, J. d'Arcy, S. Walker-Samuel, D. Hawkes, D. Atkinson, D. Collins, and M. Leach. Computationally efficient vascular input function models for quantitative kinetic modelling using DCE-MRI. *Physics in medicine and biology*, 53:1225, 2008.

[7] M. Orton, K. Miyazaki, D. Koh, D. Collins, D. Hawkes, D. Atkinson, and M. Leach. Optimizing functional parameter accuracy for breath-hold DCE-MRI of liver tumours. *Physics in medicine and biology*, 54:2197, 2009.

[8] P. Pandharipande, G. Krinsky, H. Rusinek, and V. Lee. Perfusion imaging of the liver: current challenges and future goals. *Radiology*, 234(3):661, 2005.

[9] J. Pintaske, P. Martirosian, H. Graf, G. Erb, K. Lodemann, C. Claussen, and F. Schick. Relaxivity of gadopentetate dimeglumine (Magnevist), gadobutrol (Gadovist), and gadobenate dimeglumine (MultiHance) in human blood plasma at 0.2, 1.5, and 3 Tesla. *Investigative radiology*, 41(3):213, 2006.

[10] R. Semelka, D. Martin, C. Balci, and T. Lance. Focal liver lesions: Comparison of dual-phase CT and multisequence multiplanar MR imaging including dynamic gadolinium enhancement. *Journal of Magnetic Resonance Imaging*, 13(3):397–401, 2001.

[11] P. Tofts, G. Brix, D. Buckley, J. Evelhoch, E. Henderson, M. Knopp, H. Larsson, T. Lee, N. Mayr, G. Parker, et al. Estimating kinetic parameters from dynamic contrast-enhanced T1-weighted MRI of a diffusable tracer: standardized quantities and symbols. *Journal of Magnetic Resonance Imaging*, 10(3):223–232, 1999.

[12] Y. Yamashita, K. Mitsuzaki, T. Yi, I. Ogata, T. Nishiharu, J. Urata, and M. Takahashi. Small hepatocellular carcinoma in patients with chronic liver damage: prospective comparison of detection with dynamic MR imaging and helical CT of the whole liver. *Radiology*, 200(1):79, 1996.

Table 2. *Summary table of perfusion parameters retrieve from the tumor analysis (part I). The mean tumor parameters are shown together with the corresponding standard deviation (std). The tumor mean diameter was calculated considering a perfect sphere. The calculation of the tumor dimensions considered the voxel dimensions and spacing between slices. Arterial ratio and K_L^{trans} result from fitting the equations (6) and (7) to the observed tumor voxel relative intensities. Relatively to the other parameters: Tumor Perfusion Volume is the integral of the perfusion curve; Max is the maximum of the perfusion curve; Wash-in is the maximal derivative found before the maximum. Pathology abbreviations used: Met - Metastase; NRH - Nodular Regenerative Hyperplasia; FNH - Focal Nodular Hyperplasia; Hem - Hemangioma; HCC - Hepatocellular Carcinoma.*

Patient	Tumor	Path.	Ben./Malig.	Volume (cm^3)	Diam. (cm)	Arterial ratio	std	Tum. Perf. Vol.	std	Max	std	K_L^{trans}	std	Wash-in	std
1		Met	M	35.12	4.06	0.608	0.471	7.029	12.434	0.091	0.161	0.007	0.013	0.012	0.021
2	1	NRH	B	326.33	8.54	0.202	0.206	116.097	28.977	0.739	0.179	0.071	0.024	0.037	0.015
2	2	NRH	B	3.07	1.80	0.168	0.166	117.763	23.821	0.749	0.157	0.072	0.022	0.037	0.014
3		FNH	B	6.26	2.29	0.375	0.245	152.881	25.687	1.469	0.225	0.053	0.046	0.069	0.020
4		Hem	B	17.49	3.22	0.166	0.208	263.233	46.766	3.052	0.580	0.172	0.108	0.177	0.058
5	1	HCC	M	73.28	5.19	0.660	0.422	21.683	30.749	0.233	0.337	0.013	0.015	0.022	0.024
5	2	HCC	M	0.93	1.21	0.736	0.175	147.352	35.937	1.582	0.367	0.037	0.009	0.033	0.019
5	3	HCC	M	2.40	1.66	0.755	0.211	146.286	26.811	1.565	0.241	0.039	0.010	0.042	0.036
6		HCC	M	25.11	3.63	0.514	0.362	86.182	16.684	0.785	0.154	0.027	0.026	0.055	0.020

Table 3. *Summary table of perfusion parameters retrieve from the tumor analysis (part II). The mean tumor parameters are shown together with the corresponding standard deviation (std).The tumor mean diameter was calculated considering a perfect sphere. The calculation of the tumor dimensions considered the voxel dimensions and spacing between slices. Delay and k_L result from fitting the equation (6) to the observed tumor voxel relative intensities. Relatively to the other parameters: Max time is the time at which the maximum of the perfusion curve occurs; Wash-out is the minimal derivative found after the maximum. Pathology abbreviations used: Met - Metastase; NRH - Nodular Regenerative Hyperplasia; FNH - Focal Nodular Hyperplasia; Hem - Hemangioma; HCC - Hepatocellular Carcinoma.*

Patient	Tumor	Path.	Ben./Malig.	Volume (cm^3)	Diam. (cm)	Wash-out	std	k_L	std	delay	std	Max time	std
1		Met	M	35.12	4.06	-8.51E-04	1.50E-03	0.472	0.087	2.052	2.115	69.538	8.815
2	1	NRH	B	326.33	8.54	-1.20E-03	8.45E-04	0.460	0.114	0.717	1.569	99.615	6.796
2	2	NRH	B	3.07	1.80	-1.03E-03	2.35E-04	0.461	0.111	0.342	1.100	101.370	4.157
3		FNH	B	6.26	2.29	-6.04E-03	1.64E-03	0.220	0.167	3.621	2.089	99.819	44.793
4		Hem	B	17.49	3.22	-1.30E-02	4.86E-03	0.226	0.156	3.066	2.295	94.617	8.308
5	1	HCC	M	73.28	5.19	-6.57E-04	6.79E-04	0.406	0.164	2.261	1.717	74.294	22.948
5	2	HCC	M	0.93	1.21	-1.63E-03	3.83E-04	0.103	0.008	4.804	0.483	105.036	6.176
5	3	HCC	M	2.40	1.66	-1.62E-03	2.63E-04	0.109	0.020	5.000	0.000	103.035	8.131
6		HCC	M	25.11	3.63	-6.60E-03	3.15E-03	0.172	0.138	3.954	1.916	84.067	6.478